

# Faceted Design of Channels for Low-Dispersion Electrokinetic Flows in Microfluidic Systems

Gregory J. Fiechtner and Eric B. Cummings\*

Sandia National Laboratories, P.O. Box 969, MS 9951, Livermore, California 94550

**A novel methodology for designing microfluidic channels for low-dispersion, electrokinetic flows is presented. The technique relies on trigonometric relations that apply for ideal electrokinetic flows, allowing faceted channels to be designed using common drafting software and a hand calculator. Flows are rotated and stretched along the abrupt interface between adjacent regions having differing specific permeability—a quantity with dimensions of length that we introduce to derive the governing equations. Two-interface systems are used to eliminate hydrodynamic rotation of bands injected into channels. Regions bounded by interfaces form faceted flow “prisms” with uniform velocity fields that can be combined with other prisms to obtain a wide range of turning angles and expansion ratios. Lengths of faceted prisms can be varied arbitrarily, simplifying chip layout and allowing the ability to reduce unwanted effects such as transverse diffusion and Joule heating for a given faceted prism. Designs are demonstrated using two-dimensional numerical solutions of the Laplace equation.**

Capillary electrophoresis has become a major technique for performing separations on microfluidic chips. This has led to a large number of studies that examine the consequences of the design of electrokinetic channels on analyte dispersion. Low-dispersion turns were developed during these past studies, in part, to place a long separation column into a high-density fluidic circuit. Most of these low-dispersion designs are predicated on reducing the “racetrack effect” that results from the shorter path length on the inside wall of a turn compared to that for the outside wall, complicated further by the corresponding distribution of the electric field strength.<sup>1</sup> Because comparatively narrow channels minimize this effect, a number of designs incorporate turning sections that are narrower than the straight sections of conduction channel.<sup>2–15</sup> Alternatively, designs can minimize the dispersion

by altering the channel geometry immediately after the turning section.<sup>16</sup> The racetrack effect is also reduced greatly by using turns for which the radius of curvature is large compared to the channel width.<sup>17–20</sup> Complementary pairs of turns can reduce the dispersion introduced using a single turn.<sup>20</sup> Wavy walls on the inner side of turns reduce the flow velocity there with respect to that for the outer wall.<sup>21</sup> The velocity on a channel side wall of a polymer microchannel can be increased by pretreating the wall with a pulsed, UV laser, thereby decreasing dispersion in turns.<sup>22,23</sup>

In this paper, we demonstrate a new faceted design methodology that implements results from the theory of ideal electrokinesis. Rather than address the racetrack effect directly, the technique uses abrupt changes in channel-specific permeability along lines of distinct angle to affect a flow system having a piecewise uniform velocity. The resulting technique allows the use of simple trigonometric relations to calculate the flow field, enabling algebraic optimization and dispersion minimization of electrokinetic channel designs. The methodology can be applied to generate turns of any angle and width. Moreover, the regions of

\* Corresponding author. E-mail: ebcummi@sandia.gov. Tel: 925-294-2385. Fax: 925-294-3020.

(1) Zubrisky, E. *Anal. Chem.* **2000**, *72*, 687A–690A.  
(2) Gas, B.; Kenndler, E. *Electrophoresis* **2002**, *23*, 3817–3826.  
(3) Griffiths, S. K.; Nilson, R. H. *Anal. Chem.* **2001**, *73*, 272–278.  
(4) Griffiths, S. K.; Nilson, R. H. Method and Apparatus for Reducing Sample Dispersion in Turns and Junctions of Microchannel Systems. U.S. Patent 6270641, 2001.  
(5) Molho, J. I.; Herr, A. E.; Mosier, B. P.; Santiago, J. G.; Kenny, T. W.; Brennen, R. A.; Gordon, G. B.; Mohammadi, B. *Anal. Chem.* **2001**, *73*, 1350–1360.  
(6) Molho, J. I.; Herr, A. E.; Mosier, B. P.; Santiago, J. G.; Kenny, T. W.; Brennen, R. A.; Gordon, G. B. *Solid-State Sensor and Actuator Workshop*, Hilton Head, SC, Transducers Research Foundation: Cleveland, OH, 2000; pp 132–137.

(7) Manz, A.; Bousse, L.; Chow, A.; Metha, T. B.; Kopf-Sill, A.; Parce, J. W. *Fresenius J. Anal. Chem.* **2001**, *371*, 195–201.  
(8) Gao, Q. F.; Shi, Y. N.; Liu, S. R. *Fresenius J. Anal. Chem.* **2001**, *371*, 137–145.  
(9) Kutter, J. P. *Trends Anal. Chem.* **2000**, *19*, 352–363.  
(10) Petersen, N. J.; Mogensen, K. B.; Kutter, J. P. *Electrophoresis* **2002**, *23*, 3528–3536.  
(11) Mogensen, K. B.; Petersen, N. J.; Hubner, J.; Kutter, J. P. *Electrophoresis* **2001**, *22*, 3930–3938.  
(12) Jacobson, S. C.; Ramsey, J. D.; Culbertson, C. T.; Ramsey, J. M. *Proceedings of the Micro Total Analysis Systems Symposium*, Nara, Japan, Kluwer Academic Publishers: Boston, MA, 2002; Vol. 2, pp 608–610.  
(13) Paegel, B. M.; Hutt, L. D.; Simpson, P. C.; Mathies, R. A. *Anal. Chem.* **2000**, *72*, 3030–3037.  
(14) Kopf-Sill, A. R.; Parce, J. W. Microfluidic Systems Incorporating Varied Channel Dimensions. U.S. Patent 5842787, 1998.  
(15) Fu, L.-M.; Yang, R.-J.; Lee, G.-B. *Electrophoresis* **2002**, *23*, 602–612.  
(16) Nordman, E. S. Serpentine Channel with Self-Correcting Bends. U.S. Patent 6176991, 2001.  
(17) Griffiths, S. K.; Nilson, R. H. *Anal. Chem.* **2002**, *74*, 2960–2967.  
(18) Gottschlich, N.; Jacobson, S. C.; Culbertson, C. T.; Ramsey, J. M. *Anal. Chem.* **2001**, *73*, 2669–2674.  
(19) Culbertson, C. T.; Jacobson, S. C.; Ramsey, J. M. *Anal. Chem.* **2000**, *72*, 5814–5819.  
(20) Culbertson, C. T.; Jacobson, S. C.; Ramsey, J. M. *Anal. Chem.* **1998**, *70*, 3781–3789.  
(21) Dutta, D.; Leighton, D. T. *Anal. Chem.* **2002**, *74*, 1007–1016.  
(22) Johnson, T. J.; Waddell, E. A.; Ross, D. J.; Locascio, L. E. Surface Charge Modification within Preformed Polymer Microchannels with Multiple Applications Including Modulating Electroosmotic Flow and Creating Microarrays. U.S. Patent Application 2002/0023840, 2002.  
(23) Johnson, T. J.; Ross, D.; Gaitan, M.; Locascio, L. E. *Anal. Chem.* **2001**, *73*, 3656–3661.

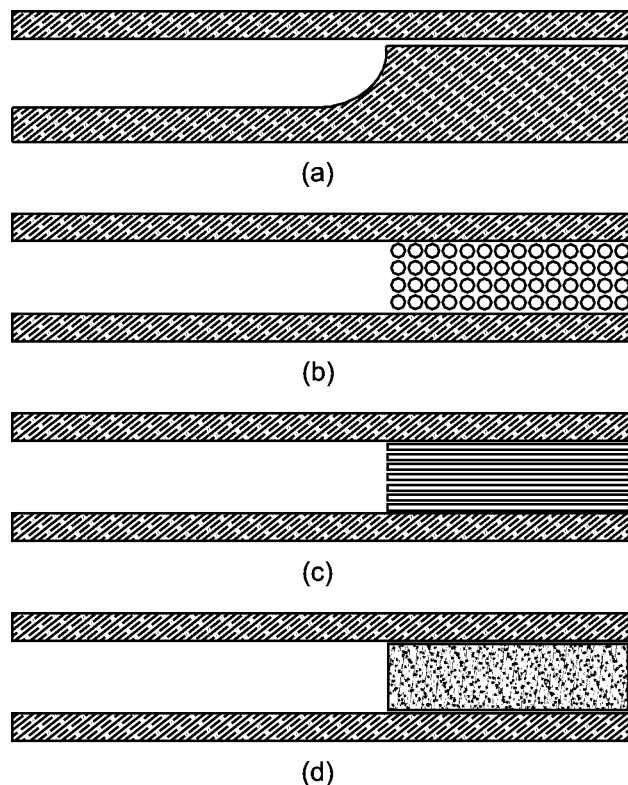


Figure 1. Methods of modifying the specific permeability  $\sigma_{sp}$  of a conduction channel: (a) multiple-depth quasi-planar open channels (side view), (b) engineered array of packing insulating posts (top view), (c) engineered array of channel-aligned insulating columns (top view), and (d) random porous or monolithic filling (side view or top view).

uniform specific permeability have a uniform velocity irrespective of the details of neighboring regions. As a result, local design features can be implemented without the need to re-design features in upstream and downstream regions.

**Interfaces for Faceted Flow Prisms.** The faceted design methods described in this paper are applicable to a number of generalized conduction problems. To illustrate the technique, and to derive the governing equations, we introduce the *specific permeability*,  $\sigma_{sp}$  (m), which has dimensions of length, in contrast to the more commonly applied *permeability*, which has dimensions of area. Here,  $\sigma_{sp}$  represents permeability per unit width. For electrokinetic flows, designs rely on abrupt changes in specific permeability along a line that forms an interface across the width of the channel. Several methods to modify the specific permeability of a channel are shown in Figure 1. In a quasi-planar channel, the specific permeability is proportional to the channel depth, which can be changed as illustrated in the channel side view of Figure 1a. Here, a two-level etch results in a channel with two distinct values of specific permeability (depth). The bottom edge of the deep region is curved at the interface—as occurs in isotropically etched channels. Alternative fabrication techniques will result in other characteristic geometries. In addition, there are other distinctly different methods to vary the specific permeability of the channels. The specific permeability can be lowered with respect to an open channel by blocking part of the channel, for example, by filling the channel with an array of posts (Figure 1b) or channel-aligned parallel columns (Figure 1c). In addition, the channel can be filled with a packing or porous medium or

pores can be generated in the substrate, as illustrated in Figure 1d. To convey their operation, channels in Figure 1b–d are shown using top views, in contrast to the side view of Figure 1a. The abrupt change in specific permeability is shown to occur along a straight line perpendicular to the channel walls defining perfect orthorhombic sections. For the channel designs discussed in this paper, the abrupt change always occurs along a line, but the angle of the line with respect to the walls can be chosen from a range of values. Each of the methods shown in Figure 1 generates characteristic levels of hydrodynamic dispersion at the interface and throughout the conduction channel and can be used separately or in combination.

## THEORY

**Ideal Electrokinetic Flow Conditions.** The design rules used to describe flow passing across an abrupt change in specific permeability result from the theory of ideal electrokinetic flow. Direct numerical simulation of electrokinetic flows requires solution of the Navier–Stokes, species transport, and electric field equations that are coupled through the charge density and material constitutive parameters, which are generally unknown. Moreover, the relevant length scales can span  $\sim 7$  orders of magnitude. Fortunately, for most cases of interest,<sup>24,25</sup> the flow approaches ideal electrokinetic conditions, and the velocity field can be computed directly from the Laplace equation without the need to solve the continuity and momentum equations. The conditions for ideal electrokinetic flow are as follows:<sup>24</sup> (1) The electric field is steady. (2) Fluid properties are uniform. (3) Channel boundaries are uniform, insulating, and impermeable. (4) The electric Debye layer is thin compared to any physical dimension. (5) Fluid velocities on all inlet and outlet boundaries satisfy the Helmholtz–Smoluchowski relation normally applicable to fluid–solid boundaries.

For these conditions, the velocity  $\mathbf{u}$  ( $\text{m s}^{-1}$ ) of the conduction fluid is everywhere proportional to the electric field  $\mathbf{E}$  ( $\text{V m}^{-1}$ )—a condition called “similitude”—such that

$$\mathbf{u} = \mu \mathbf{E} \quad (1)$$

where the coefficient  $\mu$  ( $\text{m}^2 \text{V}^{-1} \text{s}^{-1}$ ) is the mobility of the fluid. The mobility and the fluid conductivity are assumed to be constant everywhere.

**Flow Across a Single Interface.** To analyze steady fluid conduction past an abrupt change in specific permeability, we consider first the conduction channel sketched in Figure 2, having a uniform specific permeability  $\sigma_{sp1}$  (m) in region 1, left of a line of transition, and a uniform specific permeability  $\sigma_{sp2}$  in region 2, right of the line of transition. For an insulating substrate containing an electrokinetic flow, the corresponding tangential electric field is not changed by the interface. Therefore, applying conditions of similitude implied by eq 1, the tangential velocity components can be equated by writing

$$\mathbf{u}_{1o} - \mathbf{u}_{1o} \cdot \hat{\mathbf{n}} = \mathbf{u}_{2o} - \mathbf{u}_{2o} \cdot \hat{\mathbf{n}} \quad (2)$$

(24) Cummings, E. B.; Griffiths, S. K.; Nilson, R. H.; Paul, P. H. *Anal. Chem.* **2000**, *72*, 2526–2532.

(25) MacInnes, J. M. *Chem. Eng. Sci.* **2002**, *57*, 4539–4558.

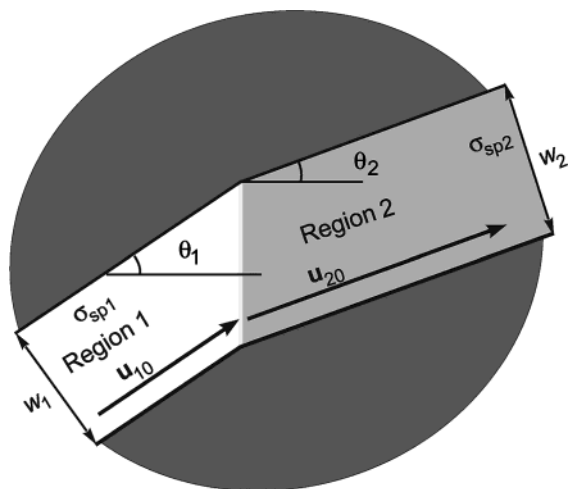


Figure 2. Sketch of a conduction channel having a single interface between regions of distinct specific permeabilities,  $\sigma_{sp1}$  and  $\sigma_{sp2}$ , channel widths,  $w_1$  and  $w_2$ , and flow angles with respect to the interface normal,  $\theta_1$  and  $\theta_2$ . The side walls of the channel are designed to satisfy the compatibility relation eq 5 such that the velocity within each region is uniform and given by eq 6. The dark gray region represents the substrate surrounding the channel.

where  $\hat{n}$  is a unit vector normal to the interface and  $\mathbf{u}_{10}$  and  $\mathbf{u}_{20}$  ( $\text{m s}^{-1}$ ) are the velocities before and after the interface, respectively. Continuity requires a constant mass flow rate  $\dot{m}$  ( $\text{kg s}^{-1}$ ) throughout the channel, such that

$$\dot{m}_1 = \dot{m}_2 \rightarrow \rho A_{c1} \mathbf{u}_1 = \rho A_{c2} \mathbf{u}_2 \quad (3)$$

where  $\rho$  is the fluid density ( $\text{kg m}^{-3}$ ) and  $A_{c1}$  and  $A_{c2}$  represent the cross-sectional areas ( $\text{m}^2$ ) immediately before and after the interface, respectively. The cross-sectional areas  $A_{c1}$  and  $A_{c2}$  share the same interface, and therefore, we may replace cross-sectional area with specific permeability, such that eq 3 becomes  $\sigma_{sp1} \mathbf{u}_1 = \sigma_{sp2} \mathbf{u}_2$ . Hence, specific permeability can be considered as permeability per unit width, and for the special case illustrated in Figure 1a, the specific permeability is equal to the channel depth. Because the tangential component of the velocity is not changed by the interface, continuity is satisfied by equating the respective velocities in a direction normal to the interface:

$$\sigma_{sp1} \mathbf{u}_{10} \cdot \hat{n} = \sigma_{sp2} \mathbf{u}_{20} \cdot \hat{n} \quad (4)$$

Equations 2 and 3 can be solved simultaneously to yield

$$\tan \theta_1 / \sigma_{sp1} = \tan \theta_2 / \sigma_{sp2} \quad (5)$$

and

$$u_{10} \sin \theta_1 = u_{20} \sin \theta_2 \quad (6)$$

where  $u = \|\mathbf{u}\|$  and  $\theta_1$  and  $\theta_2$  are the flow angles shown in Figure 2. Equation 5 is similar in appearance to Snell's law of refraction, except that tangents of the propagation angles are matched instead of sines. Equation 6 describes how the speed varies across the interface. Equation 5 or 6 can be considered compatibility

conditions for two-dimensional flow in regions 1 and 2—if a conduction–channel interface is designed to satisfy eq 5, the flow everywhere in region 1 will have a uniform velocity  $u_{10}$ ; region 2 will have a uniform flow velocity  $u_{20}$ . The channel turns the flow velocity at the interface by an amount defined to equal  $\theta_1 - \theta_2$ .

The motion of material lines through a channel is often of interest. For example, if a volume of analyte is injected<sup>26–29</sup> into an electrokinetic flow for purposes of separation, the line formed by the leading edge of the injected band defines a “material line”, and the degree of distortion of this line as it travels through a system of conduction channels is of critical importance. For the faceted designs introduced in this article, the material lines are rotated exclusively at the interface between regions of distinct specific permeability. This rotation is depicted in Figure 3a, where the dashed line represents the material line, which is shown at four instances of time— $t_1$ ,  $t_2$ ,  $t_3$ , and  $t_4$ —as it propagates through a channel. The material-line angles  $\psi_1$  and  $\psi_2$  are formed between the direction of flow and the normal to the material line for regions 1 and 2, respectively. Flow in region 1 will travel a distance  $r_1$  during a temporal interval  $t_2 - t_1$ , while flow travels a distance  $r_2$  in region 2 during the same temporal interval. The material lines shown at instances  $t_2$  and  $t_4$  can be used to draw two triangles that share a common side with a length corresponding to that of the interface, as depicted in Figure 3b. The resulting trigonometric relationships can be arranged to obtain

$$\tan \psi_2 = (\sigma_{sp1} / \sigma_{sp2}) \cos^2 \theta_1 [\tan \psi_1 + \tan \theta_1 (1 - (\sigma_{sp2} / \sigma_{sp1})^2 (1 - \tan \psi_1 \tan \theta_1))] \quad (7)$$

The widths  $w_1$  and  $w_2$  of the conduction channels in regions 1 and 2 in Figures 2 and 3 obey the relation

$$w_1 / \cos \theta_1 = w_2 / \cos \theta_2 \quad (8)$$

Therefore, the interface between channels having dissimilar specific permeabilities can be viewed as a device primitive that (1) rotates the conduction flow, (2) changes the conduction velocity/time-of-flight, (3) widens the conduction channel, and (4) rotates and deforms material lines of the flow.

**Skew-Compensated Interface Pairs.** A common design goal is a device that produces no net rotation or skew of material lines with respect to the flow direction. Any single, nontrivial interface having a nonzero incidence angle skews material lines with respect to the flow. However, if the material line is perpendicular to the flow direction initially, then  $\psi_1 = 0$ , and eq 7 simplifies to

$$\tan \psi_2 |_{\psi_1=0} = \left( \frac{\sigma_{sp1}}{\sigma_{sp2}} - \frac{\sigma_{sp2}}{\sigma_{sp1}} \right) \frac{\sin 2\theta_1}{2} \quad (9)$$

Equation 9 is symmetric about  $\theta_1 = 45^\circ$ , such that back-to-back interfaces having incidence angles that sum to  $90^\circ$  can be used

(26) Jacobson, S. C.; Hergenroder, R.; Koutny, L. B.; Warmack, R. J.; Ramsey, J. M. *Anal. Chem.* **1994**, *66*, 1107–1113.

(27) Fan Z. H.; Harrison D. J. *Anal. Chem.* **1994**, *66*, 177–184.

(28) Verpoorte, E. *Electrophoresis* **2002**, *23*, 677–712.

(29) Fu, L.-M.; Yang, R.-J.; Lee, G.-B.; Liu, H.-H. *Anal. Chem.* **2002**, *74*, 5084–5091.

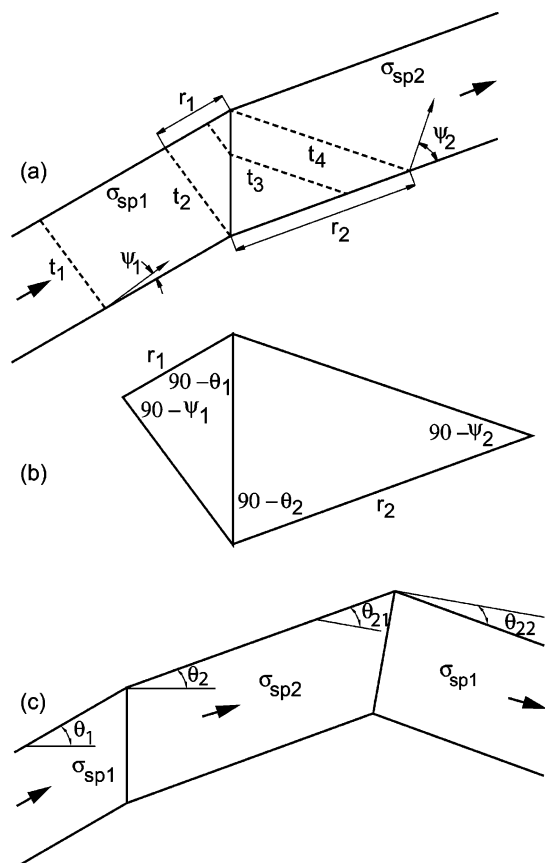


Figure 3. (a) Sketch of the conduction channel shown with four locations of a material front (dashed line) corresponding to instances  $t_1$ ,  $t_2$ ,  $t_3$ , and  $t_4$  as the front travels in the direction indicated by the large arrows. The material-line angles  $\psi_1$  and  $\psi_2$  are defined as the angle between the direction of flow and the normal to the material line in the respective sections of the channel (having relative permeabilities  $\sigma_{sp1}$  and  $\sigma_{sp2}$ ). As the material line crosses the interface in this arrangement, its angle increases with respect to the flow direction because  $\sigma_{sp1} > \sigma_{sp2}$ . The resulting length  $r_1$  traveled in section 1 corresponds to a length  $r_2$  traveled in section 2 for a given travel duration. (b) The triangles are formed by intersecting the material line at positions  $t_2$  and  $t_4$  with the channel walls in the upper illustration, where they share a common side that represents the interface. These triangles are useful for deriving an expression between the inlet and exit material-line angles (eq 7). (c) Two-interface system, used to derive expressions for two-interface, skew-compensated channels. For the specific case of a two-level etch (Figure 1a), the depth of the first and third regions will be equal ( $\sigma_{sp1}$ ). The incidence and exit angles for the second interface are defined as  $\theta_{21}$  and  $\theta_{22}$ , respectively.

to compensate for interface-induced skew or rotation of material lines. The turning angle  $\theta_T$  of such a "skew-compensated" turn is

$$\theta_T = \frac{\pi}{2} - 2\theta_1 + \tan^{-1}\left(\frac{\sigma_{sp2}}{\sigma_{sp1}} \tan \theta_1\right) - \tan^{-1}\left(\frac{\sigma_{sp2}}{\sigma_{sp1}} \frac{1}{\tan \theta_1}\right) \quad (10)$$

To derive eq 10, the overall turning angle for a two-interface system has been defined as the negative sum of the turning angles for the first and second interfaces,  $-(\theta_{T1} + \theta_{T2})$ . In addition, the exit angle of the second interface is given by  $\theta_{22} = 90^\circ - \theta_1$  (Figure 3c). There exists a trivial solution that results under the

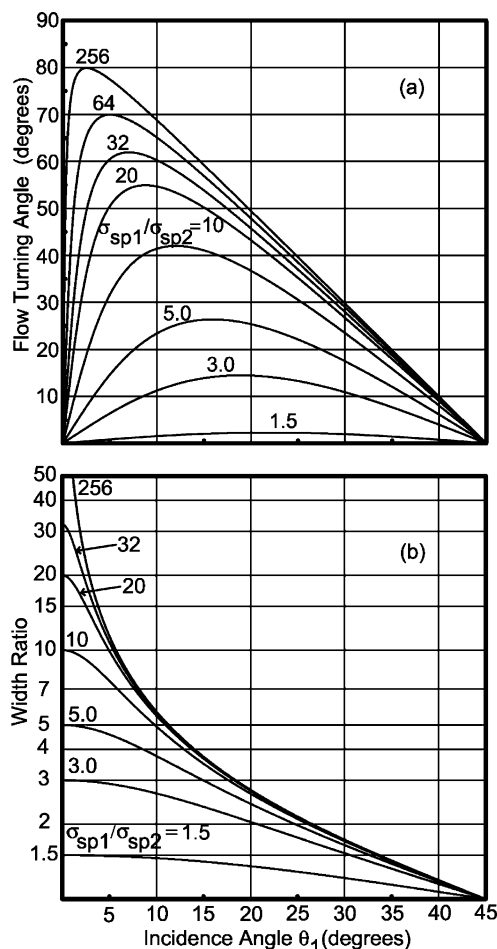


Figure 4. Turning and expanding characteristics of faceted two-interface, skew-compensated prisms: Plots versus the incidence angle of (a) the flow-turning angle and (b) the width ratio as obtained from eqs 10 and 11, respectively, for several values of the specific permeability ratio,  $\sigma_{sp1}/\sigma_{sp2}$ . As shown, the maximum turning angle for such a system is less than  $90^\circ$  and the maximum expansion is  $\sigma_{sp1}/\sigma_{sp2}$ . Larger values of turning angle and width ratio can be obtained by placing multiple faceted prisms in series.

condition  $\theta_{22} = \theta_1$  for which  $\theta_T$  is zero for all incidence angles. The resulting channel designs are flow displacers that do not rotate or expand the flow. Examples of both solutions will be presented below.

The expansion ratio of a device having back-to-back interfaces is equal to the quotient of the width ratios at the larger and smaller incidence angles. Therefore, the width ratio for a skew-compensated two-interface pair is given by the expression

$$\frac{w_{inlet}}{w_{exit}} = \left(\frac{\sigma_{sp1}}{\sigma_{sp2}}\right) \sqrt{\frac{1 + ((\sigma_{sp2}/\sigma_{sp1}) \tan \theta_1)^2}{1 + ((\sigma_{sp1}/\sigma_{sp2}) \tan \theta_1)^2}} \quad (11)$$

The flow-turning angle calculated using eq 10 and the width ratio calculated using eq 11 are plotted in graphs a and b of Figure 4, respectively. Here, it is shown that the width ratio given by eq 11 approaches unity as  $\theta_1$  approaches  $45^\circ$  and as  $\sigma_{sp2}/\sigma_{sp1}$  approaches unity. The width ratio approaches a maximum value of  $\sigma_{sp1}/\sigma_{sp2}$  as  $\theta_1$  approaches  $0^\circ$ . The maximum value of the turning angle as obtained from eq 10 is always less than  $90^\circ$ . Larger width ratios

and turning angles can be achieved by placing multiple two-interface turns in series along a channel. A two-interface, skew-compensated system that expands the channel width by a certain ratio will also shrink the channel width by an equal amount if oriented in the reverse flow direction.

## NUMERICAL METHOD

Two-dimensional simulations are accomplished using the Sandia “Laplace” code,<sup>30</sup> which is a general-purpose simulator for ideal electrokinetic flows. The software solves the modified Laplace equation  $\sigma_{sp}(x,y)\nabla\varphi(x,y) = 0$  for the velocity/electrostatic potential  $\varphi$  on a quasiplanar domain that is specified in a bitmapped image file through the field  $\sigma_{sp}$ . The uniform, square, finite-difference computational grid is generated automatically from a tagged image file bitmap whose blue channel conveys the local depth  $\sigma_{sp}(x,y)$  of the channel across the image. The blue channel is an eight-bit value for each pixel with values of 0 and 255 corresponding to a channel of zero depth—a wall—and a channel of maximum depth (specific permeability) for a given design, respectively. The solution is an exact discretization for ideal electrokinesis provided the depth of the channel does not vary along any streamlines. The discretization method enables variable-depth (specific permeability) channel geometries to be input easily using drawing programs and CAD software. Once the flow fields have been obtained, particles are “injected” and traced during postprocessing of the solution. Each particle has a vector location, velocity, scalar elapsed time, propagated distance, starting potential, and instantaneous potential, among other integrated local properties. When a particle propagates, the software updates its properties according to the bilinearly interpolated values of the fields at its location. Diffusion can be modeled by injecting a line of particles at the channel inlet and then applying a Monte Carlo scheme as the particles are tracked downstream.

Issues of the entry and exit boundary conditions were avoided earlier in the paper by assuming an infinite domain. The domain can be truncated provided the entry- and exit-flow conditions are compatible with the uniform flow in the respective regions, i.e.,

$$\mathbf{u}_i = \mathbf{u}_{i0} \quad (12)$$

and

$$\nabla\mathbf{u}_i = 0 \quad (13)$$

on the entrance to region  $i = 1$  or 2.

## RESULTS AND DISCUSSION

**Compatibility Demonstration for a Skew-Compensated Displacer.** To illustrate the effect of the compatibility condition, simulations of the speed field are shown in Figure 5 for three examples: a properly designed two-interface system (a), an improperly designed two-interface system (b), and a uniformly etched system without interfaces (c). The direction of flow is indicated by the white arrow in each image. The linear spectral color table for each simulation is shown in the lower right corner

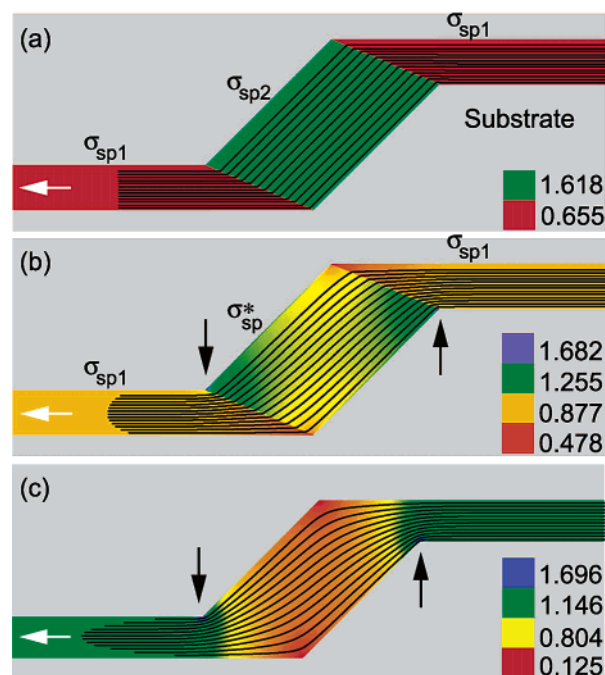


Figure 5. Numerical simulation of flow in a channel that displaces the flow with no turning angle and identical inlet and exit widths: (a) two-interface channel designed to satisfy design relations of eqs 5 and 6, (b) two-interface channel designed with specific permeability ratio in eq 5 that is twice the nominal value, and (c) channel designed with a uniform depth and no faceted interfaces. The gray region in each illustration represents the substrate. The white arrows denote flow direction within the channels. The linear color table, representing the relative speed field for each simulation, is shown in the lower right corner of each image. The inlet and exit sections ( $\sigma_{sp1}$ ) in (a) have equal uniform velocities different from the uniform velocity in the middle section ( $\sigma_{sp2}$ ), such that the color table has only two values. The specific permeability of the intermediate channel section is denoted by  $\sigma_{sp}^*$ . Local points of high speed are indicated by the black arrows for channels b and c. Superimposed streaklines are straight and parallel within each section in (a) but curved in (b) and (c). The material front exits channel a straight with no rotation. The material fronts exit channels b and c curved from hydrodynamic dispersion.

of the respective image, with blue representing the largest speeds and red representing lowest speeds—a convention used throughout this paper. The gray region represents the insulating substrate for each image. Because they are constructed using two interfaces, panels a and b of Figure 5 consist of three specific-permeability regions each: an inlet ( $\sigma_{sp1}$ ), an outlet ( $\sigma_{sp1}$ ), and an intermediate region ( $\sigma_{sp2}$ ). The specific permeability of the intermediate section is much smaller than that for the inlet and outlet, while the specific permeability of the inlet and outlet are equal for both cases a and b. For the channels fabricated using a two-level etch, the depth of the intermediate region would, therefore, be less than that of the inlet and outlet regions for cases a and b. Consequently, the speed in the intermediate region is larger than that of the inlet and outlet regions.

Compatibility is satisfied for the channel of Figure 5a, where the velocity field is uniform in each region—as shown by the uniform colors. The uniform velocities in each section for case a result in a color table with only two values. The uniform speed fields, in turn, result in a straight material line with  $\psi = 0$  at the channel exit, as shown by the superimposed streaklines. Moreover, the streaklines remain straight and parallel throughout each

(30) Cummings, E. B.; Griffiths, S. K.; Nilson, R. H. *Applied Microfluidic Physics*. LDRD Final Report; Sandia National Laboratories: Livermore, CA, 2001; SAND 2002-8018, pp 65-93.

region of the channel with abrupt rotation occurring only at the interfaces. In Figure 5b, compatibility is not satisfied for either interface because the ratio of the specific permeabilities  $\sigma_{sp1}/\sigma_{sp}^*$  is selected to be half that required by the compatibility condition (eq 5). Consequently, the speed field is not uniform within each region, particularly near the lower left and upper right corners of the middle region of low specific permeability, where locally high speeds result (the vertical black arrows point to these regions). The material line becomes noticeably curved at the exit, and the streaklines are curved substantially in the central region of the channel.

The advantages of the faceted design method are highlighted by simulating a channel that is not designed using facets, as shown in Figure 5c. Here, the conduction channel is designed with a wall geometry corresponding to that for the channels of Figure 5a and b. However, the channel of Figure 5c contains a uniform depth with no interfaces. The resulting speed field shown in Figure 5c is nonuniform, with local regions of maximum velocity approached in the regions denoted by the vertical black arrows. The corresponding material line is highly curved at the channel exit, even when compared to the performance resulting from the off-design conditions shown in Figure 5b. Hence, even a faceted channel that is designed incorrectly results in substantially less dispersion than a channel with similar geometry but designed without applying the faceted technique.

**Faceted Prisms To Turn and Expand Electrokinetic Flows.** The channel of Figure 5a represents a trivial type of faceted channel design that compensates for the skew induced by an initial interface by placing a second identical—but reversed—interface at a downstream location in the channel. The resulting flow displacer results in an unexpanded exit channel having a turning angle of  $0^\circ$ . A family of such displacers can be designed by applying the condition  $\theta_{2,2} = \theta_1$  (Figure 3c). Similarly, a family of channels can be designed to rotate and expand channels for electrokinetic flows using eq 10. A simulation of such a skew-compensated interface pair is shown in the three side-by-side images of Figure 6a, corresponding to  $\sigma_{sp1}/\sigma_{sp2} = \sim 11.57$  and  $\theta_1 = \sim 11.24^\circ$ . Here, the images represent distinct instants of a temporal sequence (denoted by  $t_1$ ,  $t_2$ , and  $t_3$ ) after particles have been injected into the flow numerically. Fluid enters the channel at the top of the figure. The material front is perpendicular to the flow velocity in the left-hand image of the figure. As shown in the middle image of Figure 6a, as the injected particles pass through the central region ( $\sigma_{sp2}$ ) after the initial interface, the material front remains straight, although it is now skewed with respect to the flow velocity (i.e.,  $\psi_2$  is nonzero). The material front is restored to a direction perpendicular to the flow velocity after passing the second interface, as is seen in the right-hand image of Figure 6a. The turn of Figure 6a forms a faceted “prism” that narrows the channel by a factor of  $\sim 4.61$  as it turns the flow velocity by  $45^\circ$ . The linear color table representing the speed field is shown in the lower right corner of the image.

The faceted design methodology is highly versatile. For example, sequences of two faceted prisms can be combined to make skew-compensated turns, as shown in Figure 6b. Here, the narrow ends of two  $45^\circ$  turns have been combined to obtain a  $90^\circ$  turn with wide inlet and outlet channels and a narrow turn interior. Because the prism orientation is the same as that for Figure 6a,

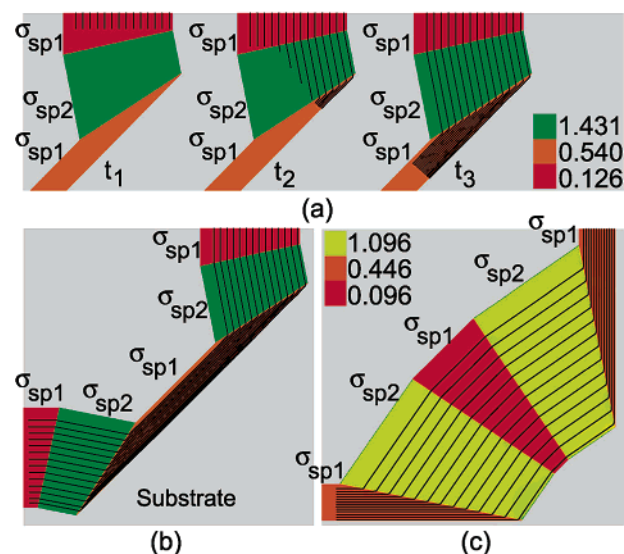


Figure 6. (a) Flow in a skew-compensated, two-interface,  $45^\circ$  turn with superimposed streaklines shown at instants  $t_1$ ,  $t_2$ , and  $t_3$ . The material line is straight and unrotated at instants  $t_1$  and  $t_3$  and is straight—but rotated—at instant  $t_2$ . The linear color table representing relative speed is displayed in the lower right corner of image a, showing three colors corresponding to the three uniform speeds characteristic of this channel design. The permeability ratio  $\sigma_{sp1}/\sigma_{sp2}$  is  $\sim 11.57$ . For the specific example of a two-level etch (Figure 1a), regions can have depths denoted by  $\sigma_{sp1}$  or  $\sigma_{sp2}$ , although turns can be constructed using any of the methods illustrated in Figure 1. Channel a forms a faceted prism that can be oriented to form a narrow  $90^\circ$  turn (b) or a wide  $90^\circ$  turn (c). The color table for (b) is the same as that for image a while the color table for (c) is shown in the upper left corner of that image. The superimposed streaklines show that the material front exits channels a–c straight and unrotated.

the color table shown applies for both panels a and b of Figure 6. If the flow is reversed for the design shown in Figure 6a, the conduction channel expands the flow by a factor of  $\sim 4.61$ . Therefore, two faceted prisms from Figure 6a that are oriented to join their wide sections can be used to construct the  $90^\circ$  turn of Figure 6c. This turn features narrow inlet and exit channels with an expanded interior. The corresponding color table is shown in the upper left corner of Figure 6c.

Channel width can be changed even more substantially by combining several faceted prisms in sequence. For example, the image of Figure 7a demonstrates faceted prisms arranged such that the entry and exit channels are parallel and each prism expands the flow channel. The resulting expansion factor is  $\sim 21.3$ . Adding an additional prism results in an expansion factor of  $\sim 98.3$  and so on. Because of the flexibility of the faceted design method, a wide range of flow-turning angles can be implemented while expanding the flow. This is illustrated in Figure 7b, where faceted prisms are combined to expand the flow channel by a factor of  $\sim 21.3$  while turning the flow by  $90^\circ$ .

**Impact of Faceted Designs on Diffusion Broadening.** For a material line that is perpendicular to the direction of flow ( $\psi = 0$ ), diffusion broadening occurs in a direction parallel to the flow along a material line of length  $w$ . For a nonzero incident angle, a single interface will always result in a nonzero material angle  $\psi$ . This results in increased diffusion broadening, because diffusion takes place in the transverse direction. For example, for the middle section of the  $45^\circ$  turn of Figure 6a, the material-line angle  $\psi_2$  is

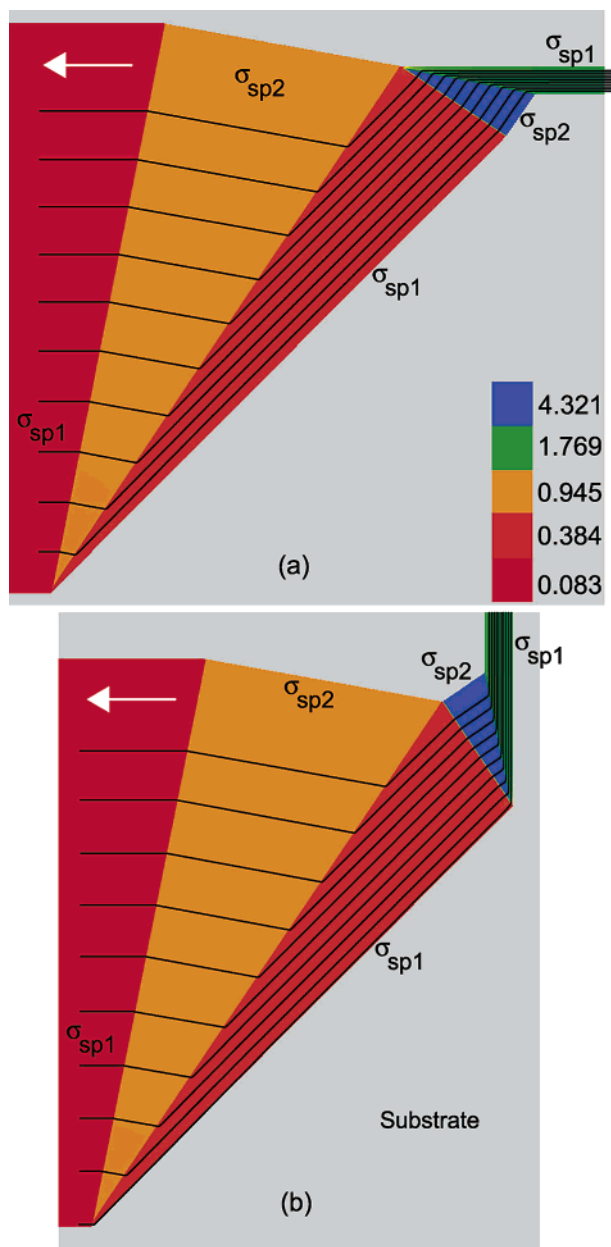


Figure 7. (a) In-line and (b) 90° turn  $\sim 21.3\times$  expanders formed by placing faceted prisms shown in Figure 6a in series. Flow exits the channels in the direction indicated by the white arrows. The linear color table shown in the lower right corner of (a) represents the relative speed field and contains five distinct values owing to the five distinct and uniform speeds characteristic of the faceted channels. The expanded material line exits the channel straight and unrotated for both examples.

$\sim 65.5^\circ$ , such that the length of the material line is increased by a factor of  $\sim 2.41$ . At the same time, stretching of the line sharpens gradients normal to the material line by a corresponding amount, producing an increase in diffusion to first order by a factor of  $1/\cos^2\psi_2 = \sim 5.81$ . The diffusion-broadened line is then rotated back to an orientation perpendicular to the direction of flow by the next interface. Designs that minimize transverse diffusion broadening can be implemented in two ways: (1) The channel length can be shortened as much as desired without impacting channel performance adversely because faceted channels have a uniform speed. (2) The local Peclet number can be increased by

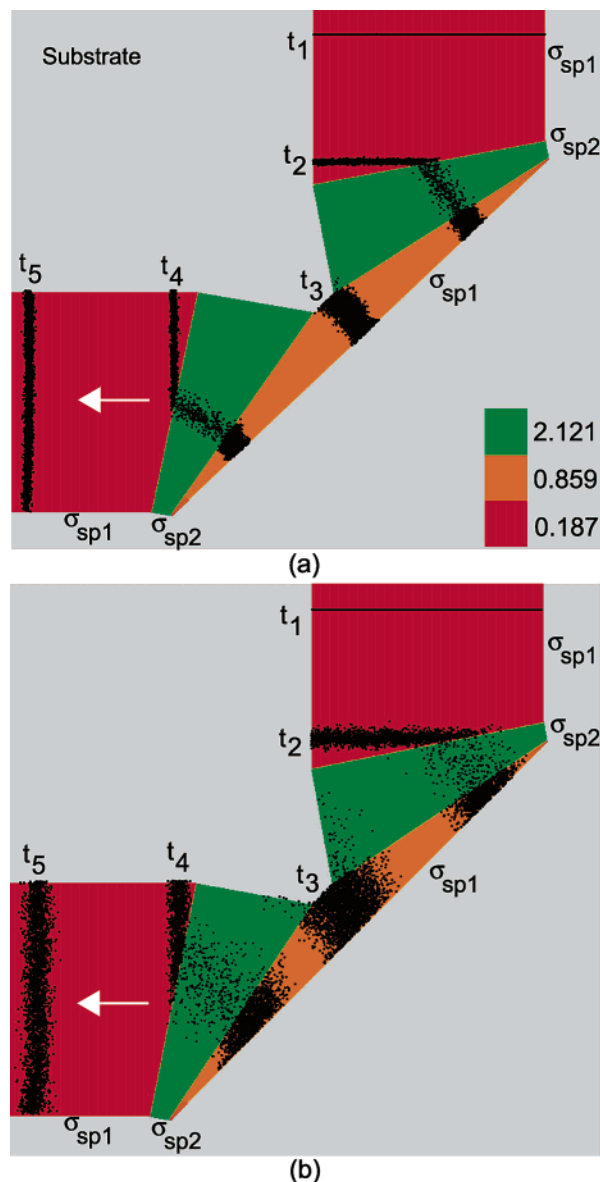


Figure 8. Simulation of the flow in the 90° skew-compensated turn of Figure 6b. Diffusion is modeled using a Monte Carlo method for distinct positions at instants  $t_1$ ,  $t_2$ ,  $t_3$ ,  $t_4$ , and  $t_5$  for an injected band as it travels through the channel in the direction indicated by the white arrow. The inlet (and exit) Peclet number is  $\sim 57.6$  for case a and  $\sim 18.4$  for case b. The interior faceted prism sections have been shortened in the direction of flow to minimize the contribution to band broadening caused by diffusion. The linear color table representing the relative speed field for both simulations is shown in the lower right corner of (a) and can be considered as an indicator of the relative Peclet number within the channel.

choosing specific permeabilities and incidence angles that combine to increase the local channel velocity.

Neither design condition can remove the influence of transverse diffusion completely. For example, if the length of a faceted section is reduced by the maximum amount, fluid must still traverse a triangular region of finite size. However, the contribution to overall band broadening from diffusion in these regions can be reduced substantially. This is demonstrated in Figure 8, where design principles 1 and 2 are used to minimize the contribution of transverse diffusion to band broadening in a faceted 90° turn similar to that shown in Figure 6b. Here, diffusion has

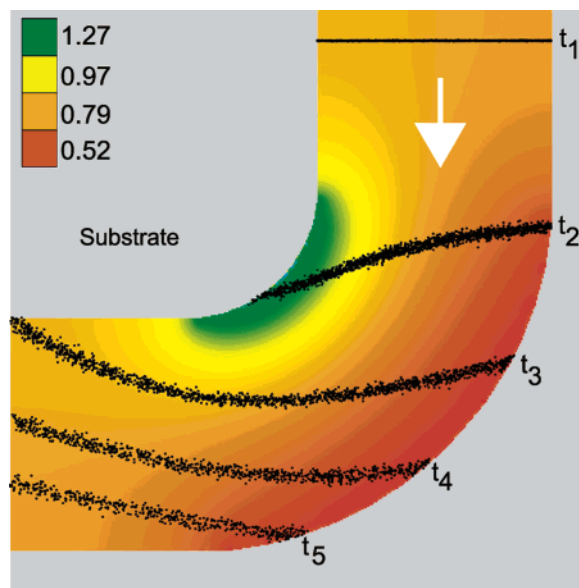


Figure 9. Simulation of the flow in a 90° turn of constant width and uniform depth. The channel width was selected to match that for the inlet and outlet faceted prisms shown in Figure 8. The velocity field is nonuniform, as indicated by the linear color table in the upper left corner of the image. A band is injected at time  $t_1$ , and the dispersion is illustrated by tracking the band downstream at instants  $t_2$ ,  $t_3$ ,  $t_4$ , and  $t_5$ . The Peclet number is  $\sim 36$ , falling between those in Figure 8. As shown, the flow dispersion is large compared to diffusion broadening, with the portion of the band nearest to the inner wall of the turn flowing off the computational domain for times  $t_3$ ,  $t_4$ , and  $t_5$ .

been included in simulations for Peclet numbers of 57.6 and 18.4 in the inlet and outlet sections of the turn. The resulting band broadening is shown in Figure 8a and b, respectively, where a band travels through the channels in the direction indicated by the white arrow, and the band appearance is shown at five distinct instances denoted by  $t_1$ ,  $t_2$ ,  $t_3$ ,  $t_4$ , and  $t_5$ . The diffusion-broadened bands are stretched and rotated at interfaces with a geometry unique to the faceted design method. This alters the appearance of bands distinctly depending on the faceted prism through which they pass, as demonstrated by comparison of bands at instants  $t_3$  and  $t_5$ , for example. The presence of diffusion does not contribute to hydrodynamic dispersion because bands exit the turn unrotated, even when the amount of diffusion is comparatively large. The length of each interior section of the turn has been reduced when compared to that for the design shown in Figure 6b. Moreover, the velocity is comparatively large in sections with nonzero material-line angle, resulting in an increase in local Peclet number by a factor of  $\sim 11.3$  over that for the channel inlet. As a result, the contribution to band broadening from diffusion in these regions is negligible compared to that occurring in the other sections of the turn.

The benefits of faceted prisms are highlighted by comparing the results of Figure 8 with the comparatively large amounts of dispersion shown in Figure 9, where a 90° turn of constant width and uniform depth has been simulated. This turn was constructed by connecting the inlet and outlet prisms for the turn of Figure 8 using inner and outer arcs. The velocity field is nonuniform, achieving a maximum value midway through the turn near the inner arc. This variation, coupled with the racetrack effect, results in dispersion that is much larger than that for the turn of Figure

8, as demonstrated by tracking an injected band at instants  $t_1$ ,  $t_2$ ,  $t_3$ ,  $t_4$ , and  $t_5$ . The Peclet number is  $\sim 36$ , intermediate to those for the simulations shown in Figure 8. The degree of band broadening caused solely by diffusion in Figure 9 is similar to that of Figure 8. However, the injected band shown in Figure 9 suffers extreme amounts of dispersion when compared to diffusion broadening, with the portion of the band near the inner wall of the turn flowing off the edge of the computational domain for times  $t_3$ ,  $t_4$ , and  $t_5$ .

#### SUMMARY AND CONCLUSIONS

The results demonstrate the utility of the faceted design technique. Faceted prisms can be designed in common drafting software using a hand calculator. Moreover, the designs are uncoupled completely: the interfaces are immune to the details of what passes before or after, as long as their compatibility conditions are satisfied locally. Once an object has been constructed, the base object can be used in combination with identical copies or with other objects to obtain any turning angle or expansion ratio. This allows complex systems to be plumbed together from simpler subsystems—for example—a 256:1 low-dispersion channel expander can be pieced together simply once a 4:1 low-dispersion prism is designed. The lengths of individual sections can be varied arbitrarily without modifying the flow characteristics of neighboring sections.

A number of design advantages result directly from the versatility of the faceted technique. Because the length of each section can be increased or decreased arbitrarily, and because the relative velocity in certain sections can also be selected during the design process, the importance of transverse diffusion can be minimized by increasing the effective Peclet number over a short distance. Moreover, for applications in which the applied potential is to be maximized, the residence time for fluid in sections with high field strength can be minimized, thereby minimizing the adverse effects of Joule heating. By careful orientation of faceted prisms and the design of their interfaces, further minimization of diffusion and Joule heating can be incorporated. For example, choice of interface angle governs the resulting rotation of the material line, which, in turn, governs the amount of transverse diffusion. The orientation of designed facets can affect practical performance. For example, the design of Figure 6c may be preferable to that shown in Figure 6b, because the central portion of the turn is much wider, and therefore, the electric field density is lower. In addition, the use of faceted prisms eliminates sharp variation in electric field strength, thereby eliminating the unwanted consequences of local "hot spots." The faceted technique also results in rapid and simple design of systems of channels on a chip, since the lengths of individual sections can be varied arbitrarily and quickly without the need to re-design the other regions of the conduction channel. Faceted prisms can simply be copied and pasted in drafting software to be used repeatedly in the same system.

The uncertainty that results from practical considerations requires further study—both by modeling and by experimental tests. There are numerous manufacturing methods to produce abrupt variation in specific permeability, each contributing to hydrodynamic dispersion in a unique way. For example, if a simple, two-level etch is employed as illustrated in Figure 1a, dispersion will be introduced in the out-of-plane direction. This dispersion is minimized for comparatively shallow and wide

channels. The physical limits of manufacturing will restrict the range of interface angles that can be implemented. Hence, the maximum expansion across a single interface is approached as the incident angle approaches the physically unrealizable value of 90°. The maximum achievable incidence angle will be determined by manufacturing methods. For example, the intersection of large-angle interfaces with channel walls will be eroded during wet-etching processes. The degree of this erosion is minimized for shallow channel designs. Further study is necessary to evaluate the impact that such manufacturing issues have on the overall system performance. In addition, because each interface will introduce dispersion, a practical upper bound on the number of interfaces will exist depending on the method used to vary the specific permeability of channel sections.

The faceted design methodology has been developed for flows that satisfy or satisfy approximately the Laplace equation and can therefore be viewed mathematically as conduction. The emphasis

of this discussion is oriented toward microfluidic design for electrokinetic systems. The emphasis on compensating for skew of material lines is intended to extend the utility of the methodology to systems that must transport analytes with minimal hydrodynamic dispersion. The methodology can also be used for electrical and thermal conductors and Darcy's law design of flow systems.

#### ACKNOWLEDGMENT

Sandia is a multiprogram laboratory operated by Sandia Corp., a Lockheed-Martin company, for the United States Department of Energy under contract DE-AC04094AL85000.

Received for review December 20, 2002. Accepted June 27, 2003.

AC0207776